Fermi National Accelerator Laboratory

FERMILAB-Pub-89/222-E
[E-740]

Study of Fast Gases, Resolutions, and Contaminants in the D0 Muon System †

J. M. Butler, D. Eartly, D. Green, H. Haggerty, S. Hansen,
S. Igarashi, H. Jöstlein, J. Li*, R. Li*, E. Malamud, P. Martin,
H. Mao*, N. Oshima, R. Yamada, and P. Xie*
Fermi National Accelerator Laboratory
P.O. Box 500
Batavia, Illinois 60510, U.S.A.

T. Marshall
Indiana University
Bloomington, Indiana 47405, U.S.A.

S. Kunori
University of Maryland
College Park, Maryland 20742, U.S.A.

M. Fortner, J. Green, D. Hedin, T. Kramer, P. Lee, A. Tseng, and S. Willis
Northern Illinois University
DeKalb, Illinois 60115, U.S.A.

Y. Antipov, B. Baldin, D. Denisov, S. Denisov, V. Glebov, and N. Mokhov
Institute for High Energy Physics
P.O. Box 35
Serpukhov
142284 Protvino, Moscow District, U.S.S.R.

November 1, 1989

† Submitted to Nucl. Instrum. Methods A.

Operated by Universities Research Association, Inc., under contract with the United States Department of Energy

November 1, 1989

STUDY OF FAST GASES, RESOLUTIONS, AND CONTAMINANTS IN THE DØ MUON SYSTEM

J.M. BUTLER, D. EARTLY, D. GREEN, H. HAGGERTY, S. HANSEN, S. IGARASHI, H. JÖSTLEIN, J. LI,* R. LI,* E. MALAMUD, P. MARTIN, H. MAO,* N. OSHIMA, R. YAMADA, AND P. XIE*

Fermi National Accelerator Laboratory, Batavia, IL 60510, USA

T. MARSHALL

Indiana University, Bloomington, IN 47405, USA

S. KUNORI

University of Maryland, College Park, MD 20742, USA

M. FORTNER, J. GREEN, D. HEDIN, T. KRAMER, P. LEE, A. TSENG, AND S. WILLIS

Northern Illinois University, DeKalb, IL 60115, USA

Y. ANTIPOV, B. BALDIN, D. DENISOV, S. DENISOV, V. GLEBOV, AND N. MOKHOV

Institute for High Energy Physics, Serpukov, USSR

Studies of the operating parameters of the DØ muon chambers are reported. The choice of operating gas was such as to find a non-explosive gas with properties similar to those of Argon-Ethane. Faster gases were also studied. The resolutions of the chambers in two coordinates were determined. Finally, systematic effects due to variations in voltage, gas mix, O_2 contamination, and H_2O contamination were determined.

---

* On leave from the Institute of High Energy Physics, Beijing, the People's Republic of China.

1. Introduction

The DØ experiment [1] is a large, general purpose, collider detector. It consists of three systems: tracking, calorimetry, and muon detection. The muon detection system is made up of a set of proportional drift tube chambers which surround large magnetized iron toroids. It features substantial protection from hadronic punchthrough by the calorimeter and an ample thickness of steel, as confirmed in test beam work [2], as well as good position resolution and solid angle coverage. An overview of the muon detection system can be found in Ref. [3]. In this paper we present systematic studies of the operating gas, the determination of the resolutions transverse and along the wire, and the effects of common contaminants on performance.

The design of the proportional tubes led to the electrostatic equipotentials shown in Fig. 1(a). What is crucial to this paper is that the drift field is 500 V/cm $< E <$ 1500 V/cm over most of the volume of the tube. Operating a prototype of this tube in Ar:C_2H_6(50:50) we previously asserted that the diffusion limited drift coordinate resolution would be 224 μm [4]. We also did prototype work on the cathode pad (Fig. 1(b)) readout electronics using anode wire time division and pad charge ratios, achieving a noise dominated resolution of $\sim 1/200$ of the pad length.

At that point in the design, production of large quantities of tubes could be begun with some confidence. Meanwhile, searches for other, safer gases, and studies of the systematics of various tube parameters could go on in parallel. This paper reports on the results of that parallel research, undertaken during the two year period of construction of the $\sim 12,000$ cell DØ muon system.

2. Studies of Fast, Non-Explosive Gases

Gases which are in common usage in drift or proportional chambers at Fermilab are Ar:C_2H_6(50:50) and Ar:CO_2 (80:20). Argon-Ethane has the virtue of high gas gain and a saturated drift velocity. The drift velocity has been measured

to be in the range 5.1 to 5.4 cm/μsec for $E \simeq 1$ kV/cm and typically varies by $\lesssim$5% for 500 V/cm $< E <$ 1500 V/cm [5]. A crude fit of the drift field $v_d(E)$ to a simple shape, $v_d(E) = v_0(1 - e^{-E/E_0})$, yields a characteristic field, $E_0 = 160$ V/cm. However, safety considerations make this gas somewhat inconvenient. Ethane also tends to break up in a high beam-flux environment and leave carbon deposits. The addition of alcohol to avoid such aging often takes some fraction of the volume of the unit cell out of saturation. For example, E_0 rises by a factor of $\simeq 3$ to 500 V/cm for only 1.5% of added alcohol. Finally, it is useful to exclude free protons from the gas in order to reduce the sensitivity of the cell to slow neutrons which are present in the high energy physics environment.

In contrast, Ar:CO_2 (80:20) is a gas with more moderate gas gain. The drift velocity at high field is v_d(E $>$ 1.5 kV/cm) $\simeq$ 5.8 cm/μsec [6]. For most field configurations this gas does not saturate, thus causing a long tail in the drift time distribution due to low field regions in the unit cell. The virtues of this gas mixture are that it is cheap, is not flammable, has no free protons, and is stable under high beam-flux. However, at higher rates in the tubes, we wish to find a gas which is faster than $\sim$5.0 cm/μsec since the time separation between hits will, at the expected future higher luminosity of the Tevatron, be less than the drift time of 1 μsec for the maximum drift distance of 5 cm.

Studies of various gas mixtures were made using a test chamber with cross section exactly as in production tubes [4], but of short length to allow easy gas changes. This cell has two potentials to vary: a wire potential V_w and a field shaping pad potential V_p. For Ar:C_2H_6(50:50) with $V_w = 5.6$ kV, $V_p = 3.0$ kV we have a gas gain $\sim 1.8 \times 10^5$ due to the 150 kV/cm field at the surface of the 50 μm diameter wire. The field is $\gtrsim$500 V/cm throughout the unit cell leading to a drift velocity everywhere within 95% of saturation.

In the test setup we used some pre-mixed bottles of Ar:C_2H_6(50:50) and Ar:CH_4 (90:10). For other mixtures we used our own gas mixing system. This system used a 1.4 liter batch tank with three inputs and one output. Each input had

a 200 cc/MIN(AIR)-Maximum flow-meter or a 50 cc/MIN(AIR)-Maximum flow-meter with a NUPRO Valve (B-4HK2) for open/close operation and a NUPRO "S" Series Fine Metering Valve for fine adjustment. In addition to these instruments, we used an Infrared Gas Analyzer (ANARAD, Inc.) to monitor the CO_2 percentage (0–25%). The setup is shown in Fig. 2.

The trigger was formed by using two scintillation counters in coincidence with cosmic rays. External tracking was provided by two PWCs with 1 mm wire pitch. The 12.8 cm width of the PWC was sufficient to cover the 10 cm drift cell. Readout was accomplished using the front end electronics developed [4] for the DØ muon chambers. The data acquisition system used an IBM/PC-XT reading a CAMAC crate (a TRANSIAC-6002 Microprocessor CAMAC Interface and a LeCroy 3512 Buffered ADC). In the off-line analysis we required a single cosmic ray by demanding a single hit for both top and bottom PWCs.

We first decided on our trial gas mixtures. A perusal of the literature [5] leads to some observations about possible two and three component gases. For Ar:CO_2 in a (90:10) mix the velocity at high fields is $v_d(\mathrm{E} > 1.0\ \mathrm{kV/cm}) \simeq 4.2\ \mathrm{cm}/\mu\mathrm{sec}$ [6] to 5.1 cm/μsec [5]. Although it is asymptotically slower than an (80:20) mix, it has a drift velocity comparable to Ar:C_2H_6(50:50), and for E >450 V/cm has $v_d > 4\ \mathrm{cm}/\mu\mathrm{sec}$. Lower concentrations of CO_2 are faster at lower fields but slower for E > 500 V/cm. A two component mixture of Ar:CH_4 (95:5) is fast at low fields, $v_d(\mathrm{E} \sim 100\ \mathrm{V/cm}) \sim 5.5\ \mathrm{cm}/\mu\mathrm{sec}$, but slow for E > 500 V/cm where $v_d <$ 3 cm/μsec. Finally, for Ar:CF_4 (90:10) the maximum velocity is $\simeq 12\ \mathrm{cm}/\mu\mathrm{sec}$, which occurs at a field of 450 V/cm. However, this gas is very field dependent; $v_d(\mathrm{E} = 2\ \mathrm{kV/cm}) \sim 6\ \mathrm{cm}/\mu\mathrm{sec}$.

Considerations of cost, safety, and high drift velocity thus led us to consider Argon with minority concentrations of CO_2, CH_4, or CF_4 in two or three component mixes. The benchmark against which to compare is Ar:C_2H_6(50:50). Data for this mix is shown in Fig. 3(a). The vertical axis is PWC position and the horizontal axes are drift time and total induced pulse height on the pads. Note

that for $V_w = 5.2$ kV and $V_p = 3.0$ kV the velocity is quite constant over the entire drift cell at $v_d \simeq 4.8$ cm/μsec indicating a roughly saturated drift velocity. The pad pulse height is fairly uniform, but with a dip at ± 2.5 cm from the wire due to a loss of ionization in a region near the pad edge (see Fig. 1(a)) where the ionization drifts to the pad and not the wire. These data verify our electrostatic calculations.

Table 1.

DRIFT VELOCITY FOR VARIOUS GAS MIXTURES

Ar	C_2H_6	CO_2	CH_4	CF_4	V_p(kV)	V_w(kV)	v_d(cm/μsec)
50	50	–	–	–	3.0	5.2	4.8
95	–	5	–	–	3.0	4.7	4.3
91.6	–	8.4	–	–	2.6	4.54	4.83
90	–	10	–	–	2.6	4.54	4.82
90	–	10	–	–	3.0	4.95	4.8
89	–	11	–	–	2.6	4.54	4.80
80	–	20	–	–	2.3	4.7	2.4
90	–	–	10	–	2.3	4.2	3.4
88	–	10	2	–	2.9	4.9	4.9
95	–	–	–	5	3.0	4.85	6.4
90	–	–	–	10	2.3	4.7	10.6
88	–	2	–	10	3.0	5.2	8.7
86	–	4	–	10	3.0	5.2	7.2
84	–	6	–	10	3.0	5.2	6.3
82	–	8	–	10	3.0	5.15	5.5
50	–	–	–	50	2.5	5.7	9.5
–	–	–	–	100	2.5	6.5	8.5

A table of drift velocities found for various test gas mixtures is included as Table 1. The benchmark gas Ar:C_2H_6 is included as well as six mixtures of Ar:CO_2, two mixtures of Ar:CO_2:CH_4, and a series of eight mixtures of Ar:CO_2:CF_4. For each mixture the wire – pad voltage, $V_w - V_p$, was varied in order to yield roughly the same gas gain as the benchmark gas. Operationally this meant varying $V_w - V_p$ until the pad pulse height looked similar to that seen in Fig. 3(a). Finally, the overall level of V_p was raised, keeping $V_w - V_p$ constant, such that the drift field over the cell was $\gtrsim$500 V/cm. For Ar:CH_4 (90:10) and Ar:CF_4 (90:10) this procedure could not be accomplished due to breakdowns. However, with CF_4 mixtures, the addition of only 2% CO_2, *i.e.* Ar:CO_2:CF_4 (88:2:10), was sufficient to meet these criteria. The data on Ar:CO_2 and Ar:CF_4 are consistent with what has been reported previously in Refs. [6] and [7].

As seen from Table 1, Ar:CO_2 (90:10) has a drift velocity, integrated over the test cell, which is comparable to the Ar:C_2H_6(50:50) benchmark. Test data for this gas mixture are given in Fig. 3(b). The data are almost indistinguishable from that of the benchmark shown in Fig. 3(a).

Faster gases were studied in three component mixtures of Ar:CO_2:CF_4. Pure mixtures of Ar:CF_4 could not achieve sufficient gas gain. The added CO_2 quencher slowed the gas slightly and hence we chose the minimum quenching mixture of Ar:CO_2:CF_4 (88:2:10). The data for V_p = 2.5 kV, V_w = 4.85 kV are shown in Fig. 3(c). The drift velocity, v_d, is $\sim$ 1.8 times faster than Ar:CO_2 (90:10), and v_d is fairly uniform over the volume of the test cell. Since the drift velocity is non-saturating [7], we took data at roughly constant gas gain ($V_w - V_p \sim$ 2.3 kV) with different drift fields; V_p= 2.0, 2.5, 3.0 kV. The global fit to a constant v_d yielded v_d = 7.6, 8.4, and 8.7 cm/μsec for these three voltages, which implies a sensitivity of $\Delta v_d/v_d \sim 3\%$ for a 10% variation $\Delta V_p/V_p$. Note that using a larger percentage of CF_4 does not lead to noticeably higher drift velocities. In fact, elevated wire voltages are needed to maintain adequate gas gain, as shown in Table 1.

We conclude that for many purposes Ar:CO_2 (90:10) will perform as a rugged drift gas with adequate gas gain and reasonably constant drift velocity. This gas is stable in high-flux environments and should be insensitive to neutron backgrounds. It is safe and cheap. In higher speed applications Ar:CO_2:CF_4 (88:2:10) is a factor 1.8 faster but otherwise behaves very similarly to Ar:CO_2 (90:10) and shares similar virtues with the exception of cost.

3. Resolutions in the Drift and Pad Coordinates

The relationship between the induced charge ratio on the pads, δ, and the position along the wire was mapped out using the external PWC shown in Fig. 2. For a given wire charge, a pad charge is induced which depends on the solid angle subtended by the pads. A very approximate result, valid for an infinitely long strip with small subtended angle, but normalized to the maximum observed value of δ is:

$$\begin{aligned} \delta &\equiv (Q_1 - Q_2)/(Q_1 + Q_2) \\ &\simeq (0.69)(4X/L) - 0.14 \end{aligned} \tag{1}$$

where X is the position along the wire and L is the repeat length (60.96 cm in this cell, see Fig. 1(b).) The normalization in Eq. 1 is given for X in the range $-L/4 < X < L/4$.

The precise relationship between the PWC determined position and the pad charge ratio is shown in Fig. 4. Also indicated in that figure is the linear relationship (Eq. 1). The rough agreement of data with the linear plot indicates that it is a reasonable first approximation. The spread of the points is an indication of the resolution. In Fig. 5, we show a fit to the residuals of observed position obtained from the pad charge ratio minus the PWC prediction, indicating a resolution of ± 2.7 mm which is $\pm 1/226$ of the repeat length L and $\pm 1/2040$ of the total drift tube length. This result is comparable to that which we have previously reported [4].

The measurement is noise dominated and in the linear approximation (Eq. 1) corresponds, in the best case of $\delta = 0$, to a measurement of the two pad charges with an accuracy of 1.7%. Note that the real noise is rather less than this since the linear approximation breaks down at the turning points where $|\delta|$ is maximal (see Fig. 4), and the quoted resolution is that integrated over a uniformly illuminated unit cell.

The drift velocity was determined by again reconstructing tracks with the two PWC's and comparing the projected track position in the PDT cell to the measured drift time. The resulting drift time to distance relationship is shown in Fig. 6, where one pixel size corresponds to 0.8 mm in space. The PWC resolution was ± 0.3 mm or almost one pixel. A linear time to distance relation is a reasonable first order fit. The slope of that fit was quoted as v_d in Table 1 for all the trial gas mixtures.

A more complicated fit was performed to account for non-linearities, of order ± 0.4 mm, in the space-time relation. A second order polynomial relation between drift time and position Z yielded an adequate value for the χ^2. In order to determine the intrinsic drift time resolution, only the three drift cells shown in Fig. 2 were used and not the coarser PWC data. We measured the three coordinates in the drift direction Z_{top}, Z_{mid}, and Z_{bot} from the three layers. These three coordinates have a common reference origin and should be equal. The residual R was defined to be $\mathrm{R} \equiv Z_{mid} - (Z_{top} + Z_{bot})/2$, with an error $\delta \mathrm{R}^2 = \delta Z_{mid}^2 + (\delta Z_{top}^2 + \delta Z_{bot}^2)/4$. A fit to the residual distribution, shown in Fig. 7, gives $\delta \mathrm{R} = 0.38$ mm. The single cell resolution can be unfolded if we assume equal errors, *i.e.* $\delta Z = \delta Z_{top} = \delta Z_{mid} = \delta Z_{bot}$, yielding $\delta Z = \sqrt{2/3}\, \delta \mathrm{R} = \pm 0.31$ mm. If the simple linear space-time relationship is assumed, the resolution becomes degraded to ± 0.38 mm. The quoted resolution of ± 0.31 mm is close to the expected diffusion limit [8] of ± 0.225 mm.

4. Systematic Parameter Variations

For the studies described in sections *4.1* and *4.2*, the gas used was Ar:CO_2 (90:10).

4.1 High Voltage

The gas gain, G, is expected to vary with reduced field, E/P, as [9]:

$$\begin{aligned} G &\simeq Ke^{\alpha a}, \text{ where} \\ \alpha/P &= Ae^{-BP/E}. \end{aligned} \tag{2}$$

In Eq. 2, α is the inverse of the mean free path for ionization known as the first Townsend coefficient, a is the wire radius, and P is the pressure. Using the fit for Argon gas quoted in Ref. 9, A = 14/(cm-Torr) and B = 180V/(cm-Torr), with $\sim$ 112 kV/cm field at the wire, one finds α = 3137/cm. For a gas gain $G \simeq 1.8 \times 10^5$ [4], and $\alpha a = 7.8$ (for 50 μm diameter wire), $K \simeq 71$.

The relative gain was tracked by measuring the pad pulse heights. Sample data taken using ^{241}Am and ^{55}Fe sources as a function of the wire high voltage are shown in Fig. 8. Clearly, the gas gain depends strongly on the wire to pad voltage difference as was previously assumed. The gain is measured to be exponentially related to this difference with coefficient 4 kV^{-1}, *i.e.* a change of $V_w - V_p$ of 250 volts causes a gain change of e. Using the approximate expression $E \sim V_0/a\ln(b/a)$, valid for a coaxial, cylindrical geometry, with $V_0 \equiv V_w - V_p$ = 1.94 kV, $b \sim 2.5$ cm = wire to pad distance, and the parameters in Eq. 2, we predict that the voltage swing that would cause a gain shift of a factor of e is

$$\frac{dV_0}{V_0} = \frac{1}{(\alpha a)(BP/E)} \tag{3}$$

yielding $dV_0 = 204\ V$, in reasonable agreement with the data.

The drift velocity is expected to be mainly dependent on the drift field, which is related to V_p. We took data over a wide range of V_p, keeping $V_w - V_p$ constant. The drift velocities vs. V_p for Ar:CO_2 (90:10) are shown in Fig. 9.

Ar:CO_2 (90:10) is not saturated but is relatively insensitive to changes in V_p, $(\Delta v_d/v_d)/V_p \approx 12\%/\text{kV}$. This slope is consistent with that reported in Ref. [6] for fields 500 V/cm $< E <$ 1500 V/cm.

4.2 Pressure

Clearly, the gain also depends on pressure. The pressure dependance of the gain was measured by varying the depth of the exhaust gas line in a 1.5 m tall, oil-filled bubbler. Data was taken using an ^{55}Fe source, with the current on the sense wire used as a measure of the gain. The results are shown in Fig. 10 where the gain is seen to decrease linearly with pressure.

From Eq. 2, one expects the gain to track the pressure as:

$$\frac{dG}{G} \simeq \frac{dP}{P}\left[\alpha a\left(1-\frac{BP}{E}\right)\right]. \tag{4}$$

Using the parameters derived in the previous section, $dG/G \simeq -1.7\ dP/P$ for $P \simeq 1$ atmosphere. This result is within a factor of ~ 2 of a linear fit to the data, which is acceptable agreement given the approximations. The measurement indicates that, in the roughly $\pm 3\%$ range of atmospheric pressure variations, the gain will change by less than $\pm 20\%$ which corresponds to a change in V_w of ± 46 volts. In DØ the barometric pressure will be continuously monitored, and perhaps used as a feedback input to the high voltage system so as to maintain constant gain.

4.3 Gas Mixture

The response of the muon chambers to variations in parameters can be observed as effects on the gain, drift velocity, or mean pulse height as a function of drift distance. Obviously, all three indicators can be mimicked by variations in the voltages V_w and V_p. We have already indicated the dependence of gain and drift velocity on applied voltages.

Data were taken with three different gas mixtures near Ar:CO_2 (90:10) in order to measure the gas gain and the drift velocity sensitivity. Figure 11 shows

the relatively large gain sensitivity (40% mean gain change between 8.4% and 11.0% CO_2). To set the scale, a 1% CO_2 change makes a 17 $\pm$ 5% gain change which is equivalent to a voltage change in V_w of about 40 volts. Note that since we measure a charge ratio (see Eq. 1), we are insensitive to gain changes in the determination of position along the wire. Furthermore, as long as we are well above discriminator threshold, any gain change will have only a minor effect on the drift time measurement.

The drift velocity for the three mixtures was relatively insensitive to mixture. Table 1 shows that v_d peaks about Ar:CO_2 (90:10) and falls off for higher and lower fractions of CO_2. At Ar:CO_2 (90:10) the slope was $\Delta v_d = -(0.01 \pm 0.01)$ cm/μsec per 1% CO_2 change although the data were also consistent with no change within the errors. In DØ we plan to control the CO_2 fraction to $\lesssim 0.1\%$ so that the effect of mixture on v_d, which is already small, will be kept negligible.

In comparison, Ar:CO_2:CF_4 was more sensitive to mixture (see Table 1). Keeping the CF_4 fraction fixed at 10%, the slope was $\Delta v_d \simeq -0.5$ cm/μsec per 1% CO_2 change for CO_2 fraction near 5% where $v_d \simeq 6.7$ cm/μsec.

5. Effects of Contaminants

Finally, the effect of common contaminants was studied. Recalling [10] that the electron attachment times are roughly 0.19 μsec for O_2 and 0.14 μsec for H_2O, it is clear that, with a drift time of 1 μsec, a 1% level of these contaminants would be very noticeable. The gas mixture was Ar:CO_2 (90:10) for all tests discussed in this section.

5.1 O_2

Oxygen contamination tests were performed at 150, 560, 1300, 2200, and 3200 ppm of oxygen with V_w= 4.54 kV and V_p= 2.6 kV. In Fig. 12, we show the pulse height relative to the data at 150 ppm (*i.e.* no O_2) as a function of drift distance. There is a drop of $\approx$ 35% in effective gas gain near the wire at 3200 ppm O_2. As we see from Fig. 8, that drop could be mimicked by a drop

in V_w of about 110 volts. However, there is more than a factor two loss in pad pulse height at 5 cm drift distance, indicating attachment of the ionization. Clear attachment effects are seen, which can be used to distinguish voltage variations from changes in gas contamination. The occurrence of a simultaneous drop of V_w and V_p which might mimic this effect is most unlikely. In any case, the O_2 level will be monitored and logged in DØ.

The effects of O_2 on the drift velocity were small. We found that $\Delta v_d = -(0.02 \pm 0.01)$ cm/μsec per 1000 ppm O_2 contamination.

5.2 H_2O

During this study, we again set V_w= 4.54 kV and V_p= 2.6 kV. The H_2O contamination was controlled to be 90, 1000, 2000, and 3000 ppm. The observable effects of H_2O are rather different from that of O_2 even though both are electronegative impurities with roughly equal attachment times.

The global drift velocity was observed to decrease fairly linearly with increasing H_2O with a fitted slope of $\Delta v_d = -(0.30 \pm 0.01)$ cm/μsec per 1000 ppm contamination. Using the results quoted in Section 4, this change in v_d for 1000 ppm H_2O is equivalent to that caused by a pad voltage variation of $\Delta V_p \simeq$ 450 volts.

Figure 13 shows the drift time vs. drift distance for 3000 ppm of H_2O. Comparing to Fig. 6, we can see that not only is the overall drift velocity reduced, but significant non-linearities have been introduced by the presence of H_2O. Looking at Fig. 13 for 2.5 cm $< |Z| <$ 4 cm and recalling the electrostatics shown in Fig. 1(a), one infers that the non-linearities are due to a decrease in v_d for the low field parts of the unit cell in the presence of H_2O.

In Fig. 14, we show the mean pad charge as a function of H_2O contamination. We note only small changes for $\lesssim$1000 ppm H_2O, with a slow falloff thereafter. At 3000 ppm H_2O, the effective gas gain has only fallen 18%. Utilizing Eq. 2 or Fig. 8, this effect could be mimicked by a supply voltage variation of $\Delta V_w \simeq$ 41 volts.

Finally, we looked for the effects of electron attachment. For the data shown in Fig. 12, there was a differential drop of 38% for 5 cm drift at 3200 ppm O_2. In contrast, 3000 ppm H_2O caused only an 11% drop. It appears from all the data that a careful monitoring of the shape of the drift velocity is the best way to track H_2O contamination, while a detailed study of the pad charge as a function of drift distance is the best way to tag O_2 contamination.

Acknowledgements

We are indebted to R. Cantal, K. Kephart, J. Sasek, and G. Sellberg for their technical support.

REFERENCES

1. Design Report, the DØ Experiment at the Fermilab Antiproton-Proton Collider (1984).
2. D. Green *et al.*, Nucl. Instr. and Meth. A244 (1985) 356.
3. C. Brown *et al.*, Nucl. Instr. and Meth. A279 (1989) 331.
4. D. Green *et al.*, Nucl. Instr. and Meth. A256 (1987) 305.
5. A. Peisert and F. Sauli, CERN 84-08 (1984).
6. C. Ma *et al.*, MIT Technical Report 129 (1982).
7. L.G. Christophorou *et al.*, Nucl. Instr. and Meth. 163 (1979) 141.
8. F. Puiz, Nucl. Instr. and Meth. 205 (1983) 425.
9. S.A. Korff, Electrons and Nuclear Counters, Van Nostrand, New York (1946).
10. S.C. Brown, Basic Data of Plasma Physics, MIT Press, Cambridge, Mass.

FIGURE CAPTIONS

1) Electrode structure of the DØ muon tubes. (a) Equipotential contours. (b) Cathode pads, showing the inner and outer electrode structure.

2) Gas test setup. A three component gas mixing tank is used. The cosmic ray trigger is formed using scintillators top and bottom. Tracking is done using PWCs top and bottom.

3) Drift time and total pad pulse height vs. coordinate position for (a) Ar:C_2H_6(50:50), (b) Ar:CO_2 (90:10), (c) Ar:CO_2:CF_4 (88:2:8).

4) Charge ratio as a function of position along the wire. Also shown is a linear relationship between position and charge ratio.

5) Residuals for the pad charge ratio. The two PWC measurements (1 mm wire spacing) were used to predict the position along the wire with negligible error.

6) Drift time as a function of the distance from the wire. The straight line is a first trial function.

7) Spatial resolution as determined for the three drift time measurements.

8) Mean total pad pulse height using ^{55}Fe and ^{241}Am sources as a function of V_w for several V_p.

9) Drift velocity as a function of pad voltage with roughly constant gas gain for Ar:CO_2 (90:10).

10) Sense wire current as a function of gas pressure.

11) Pad pulse height distribution for different gas compositions near Ar:CO_2 (90:10).

12) Relative mean pad pulse height as function of distance from the wire for different oxygen contamination fractions 150, 560, 1300, 2200, and 3200 ppm.

13) Drift time as a function of drift coordinate for Ar:CO_2 (90:10) with 3000 ppm H_2O contamination.

14) Mean pad pulse height as a function of H_2O contamination for Ar:CO_2 (90:10).

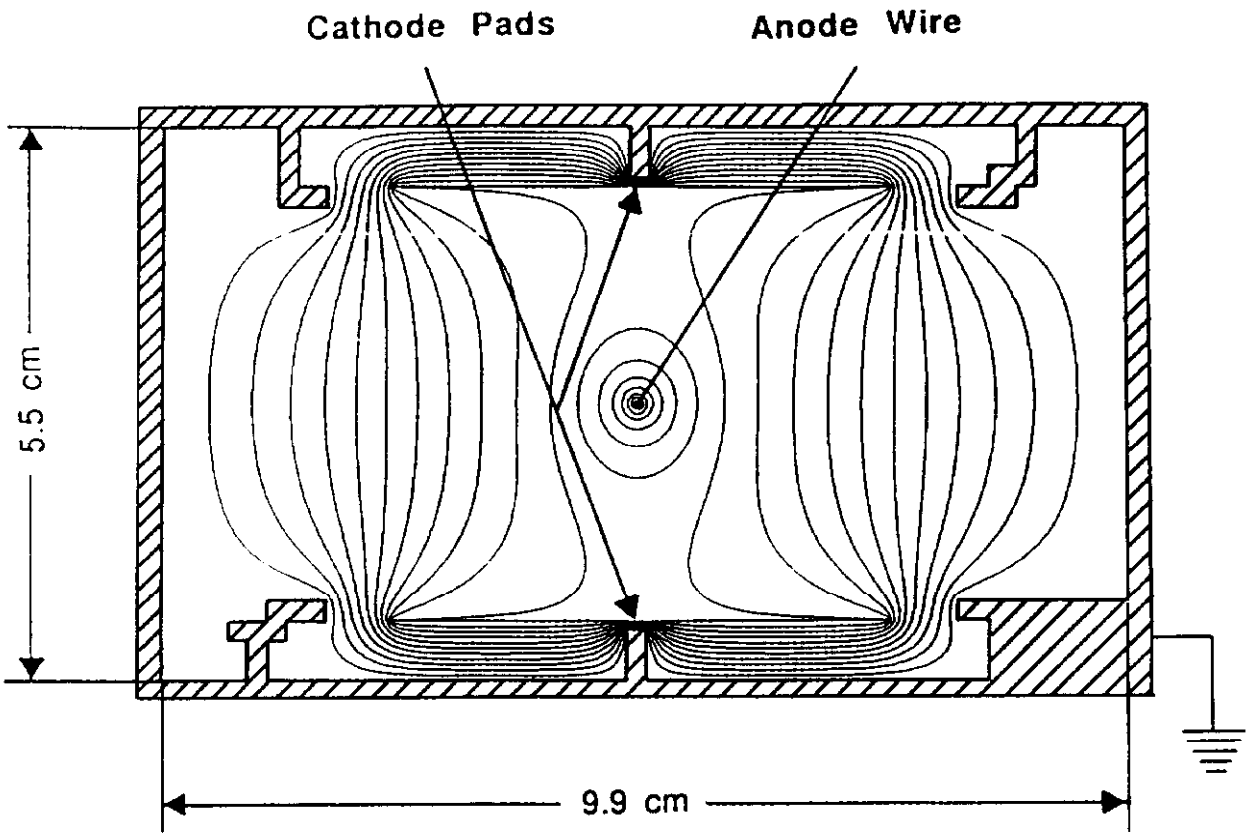
Cathode Pads
Anode Wire
5.5 cm
9.9 cm

(a)

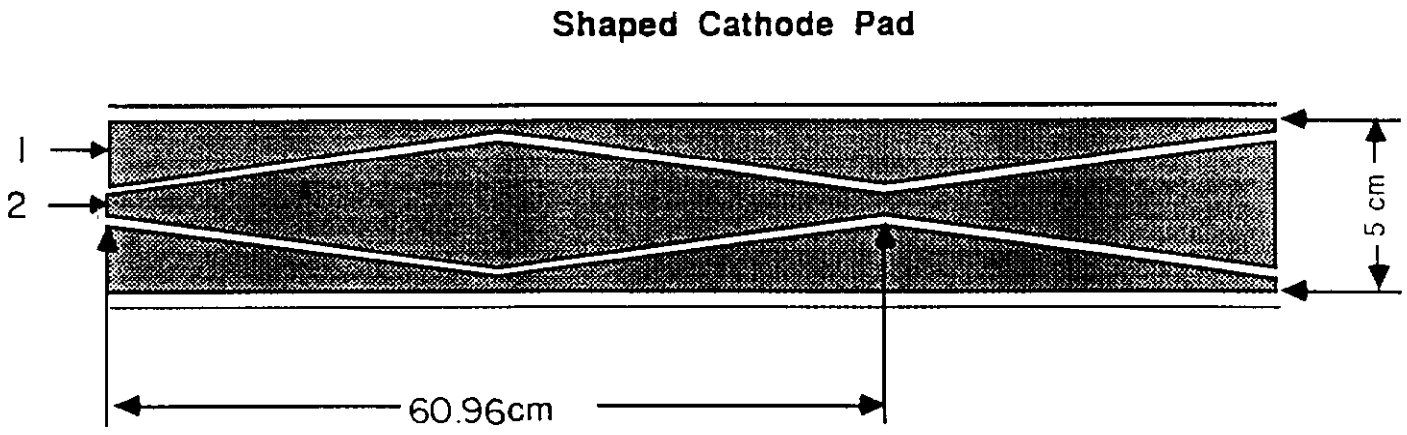
Shaped Cathode Pad
1
2
5 cm
60.96cm

(b)

Figure 1.

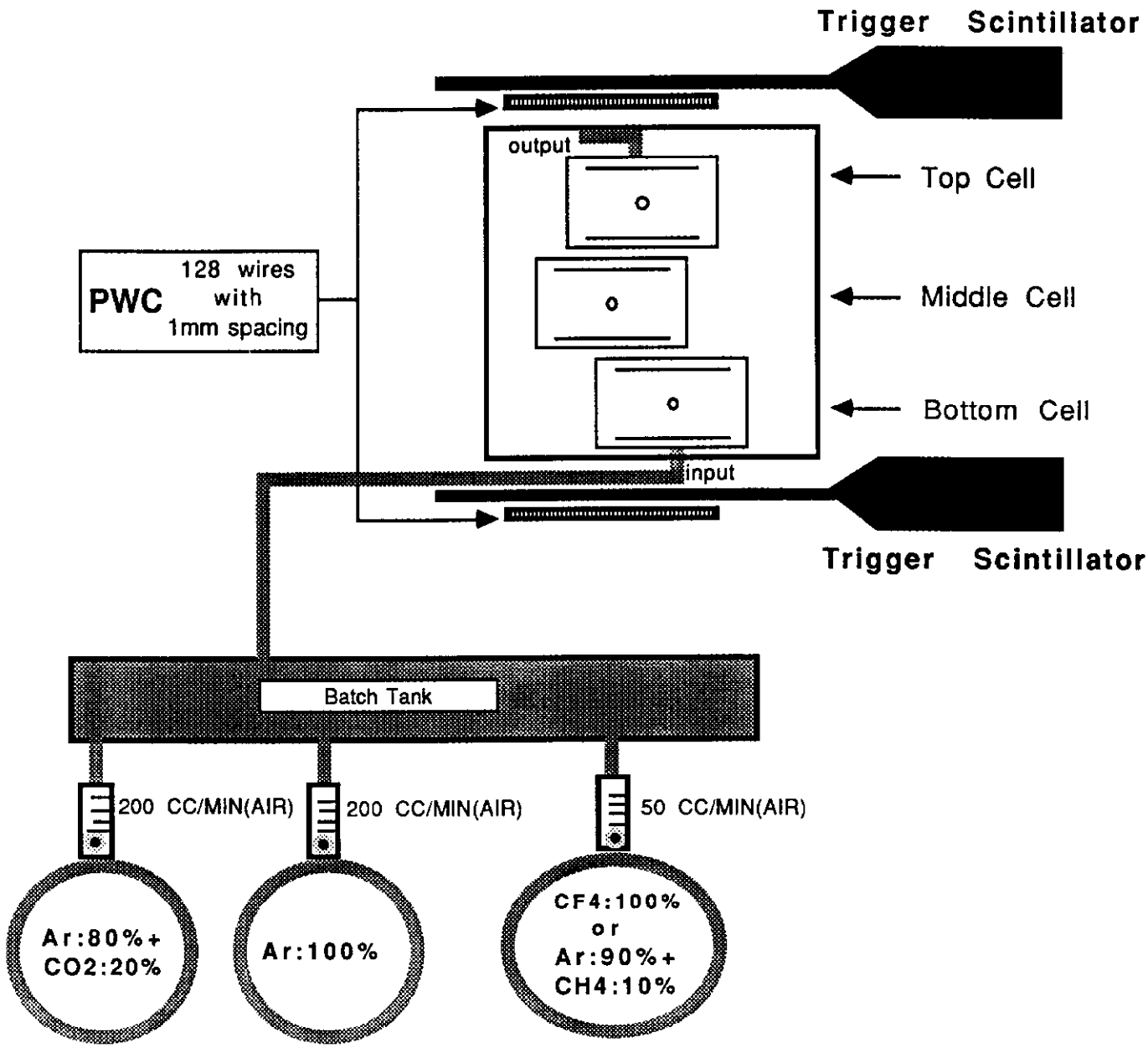
Trigger Scintillator
output
Top Cell
PWC
128 wires
with
1mm spacing
Middle Cell
Bottom Cell
input
Trigger Scintillator
Batch Tank
200 CC/MIN(AIR)
200 CC/MIN(AIR)
50 CC/MIN(AIR)
Ar:80%+
CO2:20%
Ar:100%
CF4:100%
or
Ar:90%+
CH4:10%

Figure 2.

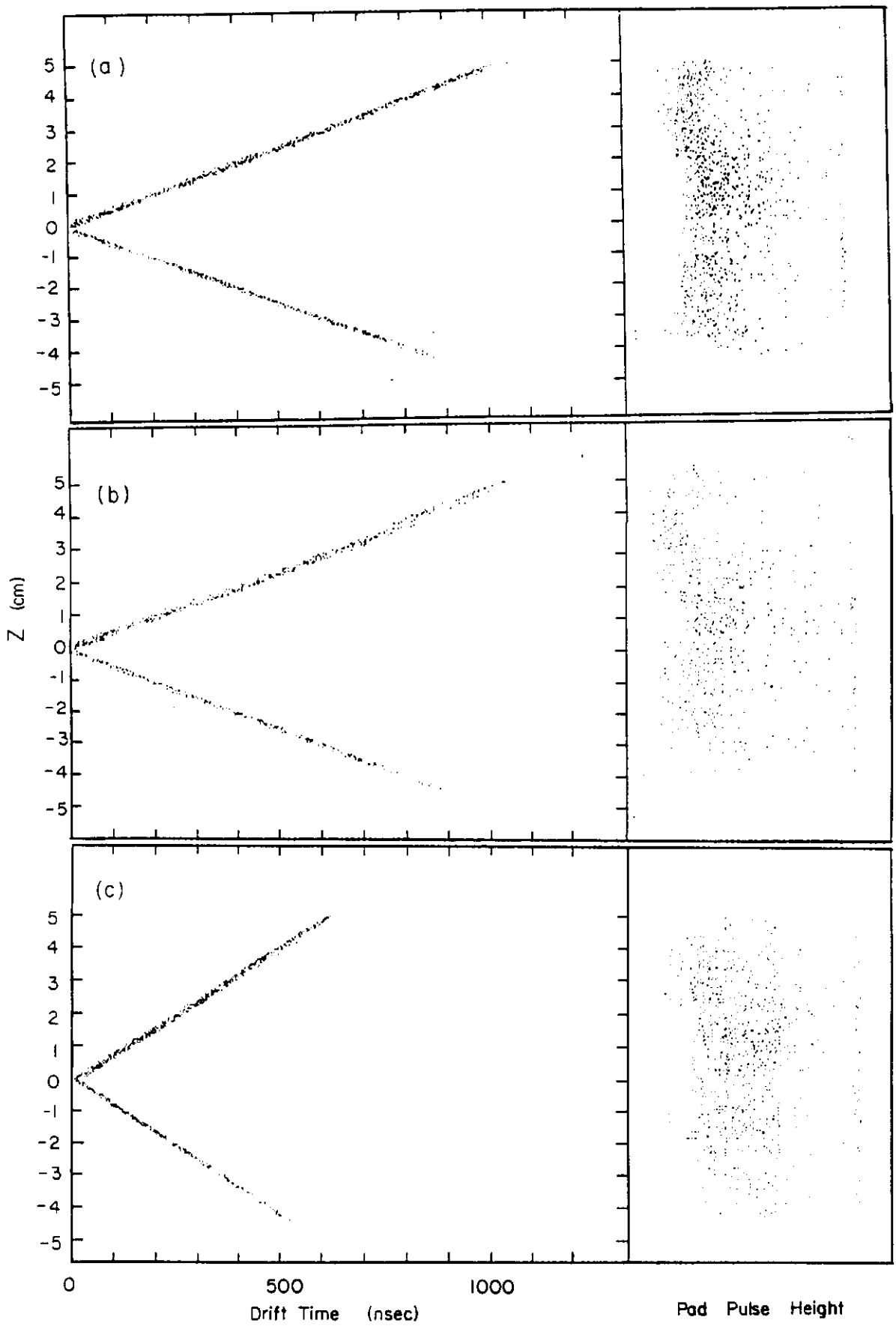
(a)
(b)
(c)
Z (cm)
5
4
3
2
1
0
-1
-2
-3
-4
-5
0
500
1000
Drift Time (nsec)
Pad Pulse Height

Figure 3.

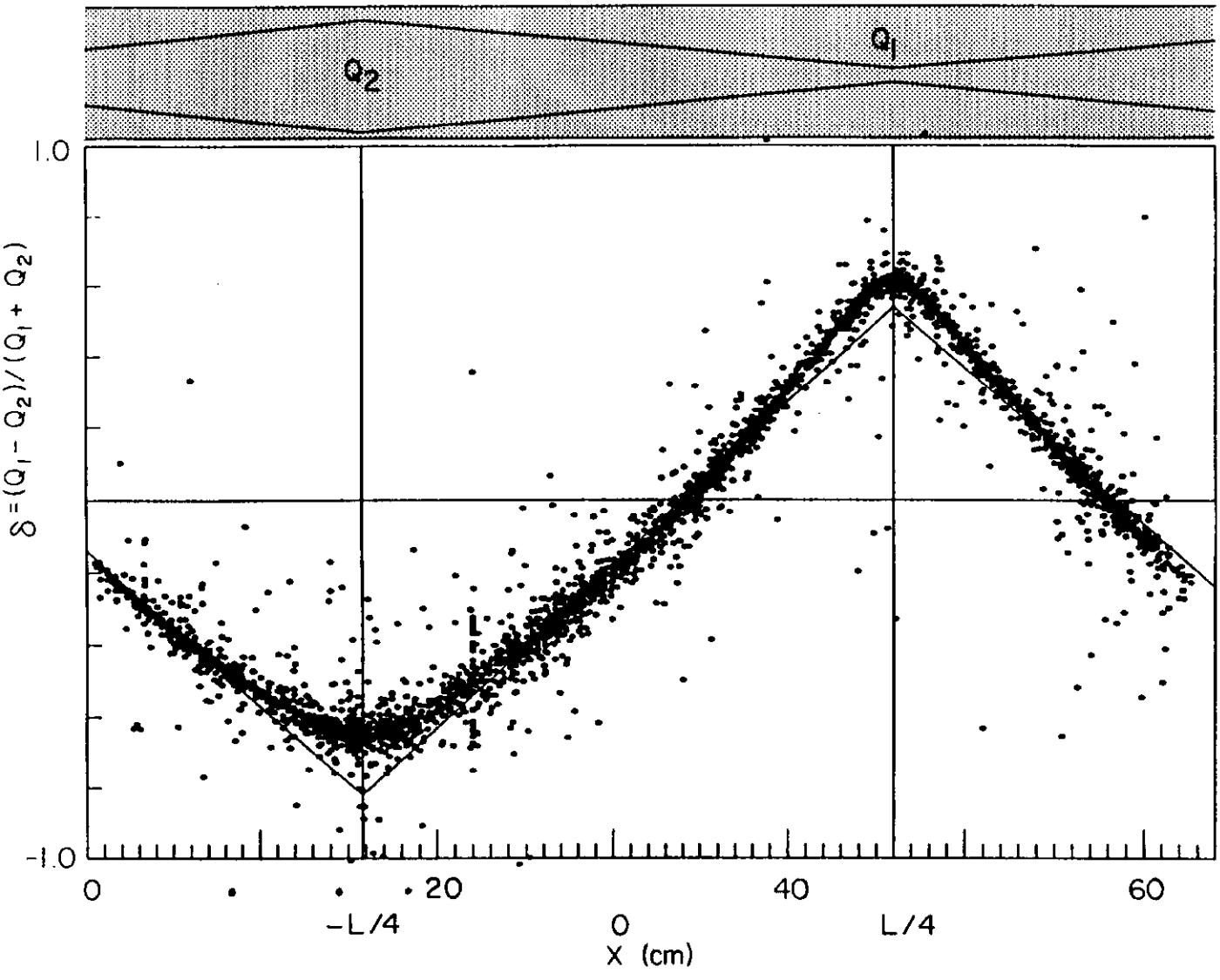

Figure 4.

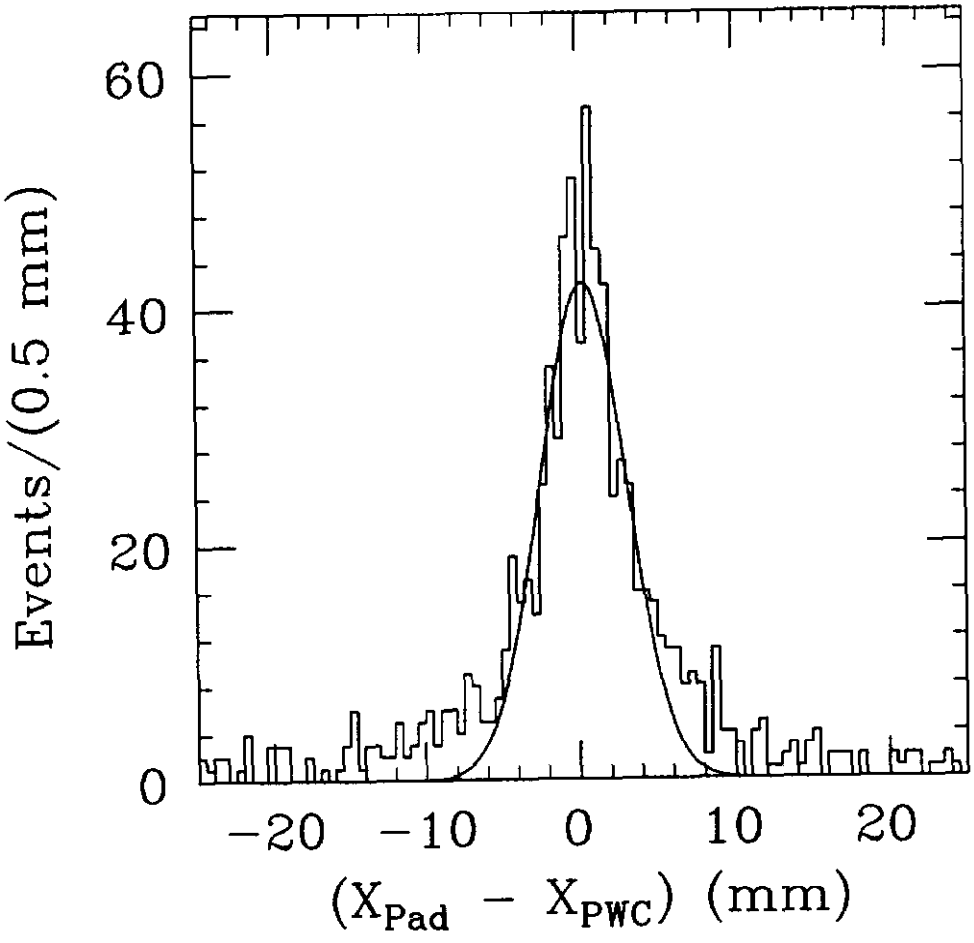

Figure 5.

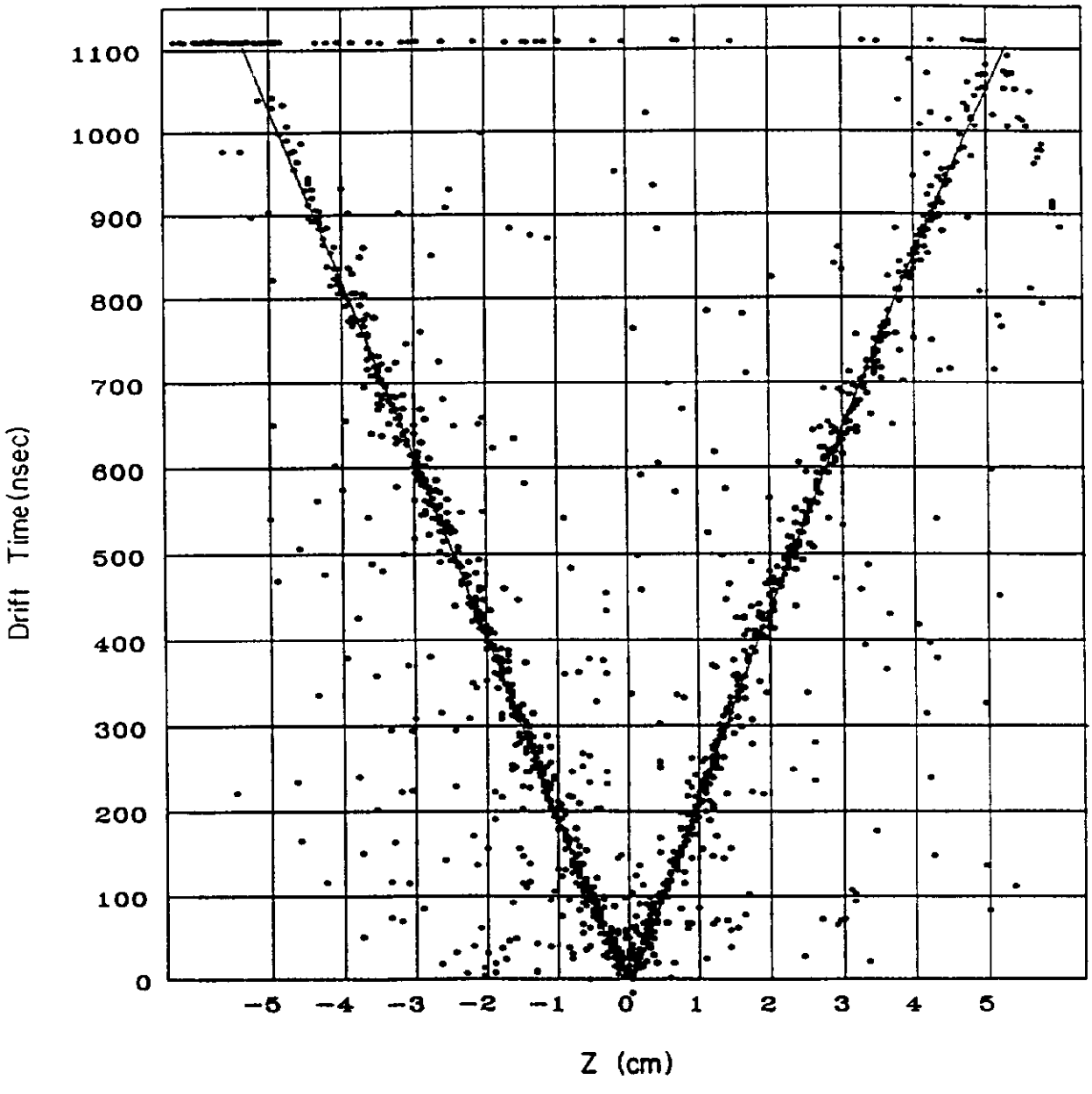
1100
1000
900
800
700
600
500
400
300
200
100
0
Drift Time (nsec)
−5
−4
−3
−2
−1
0
1
2
3
4
5
Z (cm)

Figure 6.

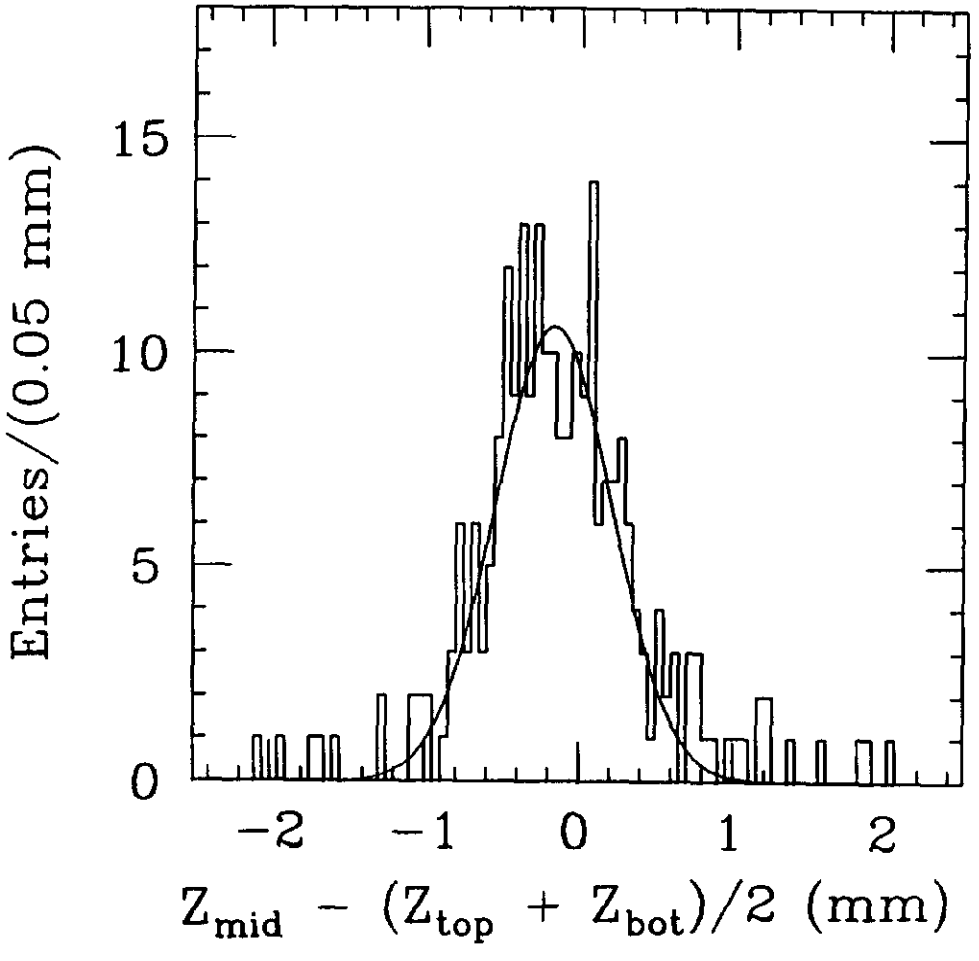

Figure 7.

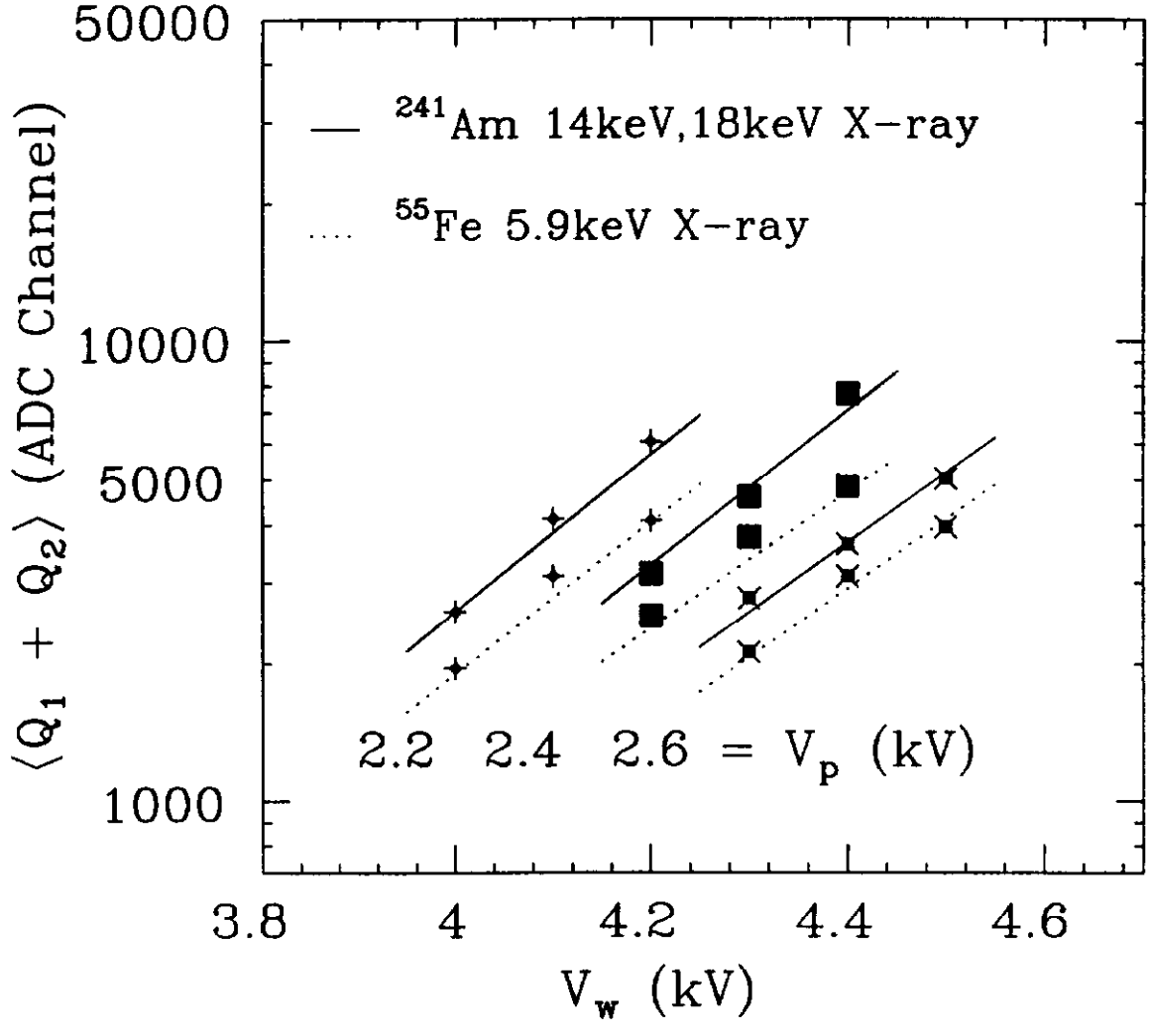
50000
10000
5000
1000
$\langle Q_1 + Q_2 \rangle$ (ADC Channel)
^{241}Am 14keV,18keV X-ray
^{55}Fe 5.9keV X-ray
2.2 2.4 2.6 = V_p (kV)
3.8
4
4.2
4.4
4.6
V_w (kV)

Figure 8.

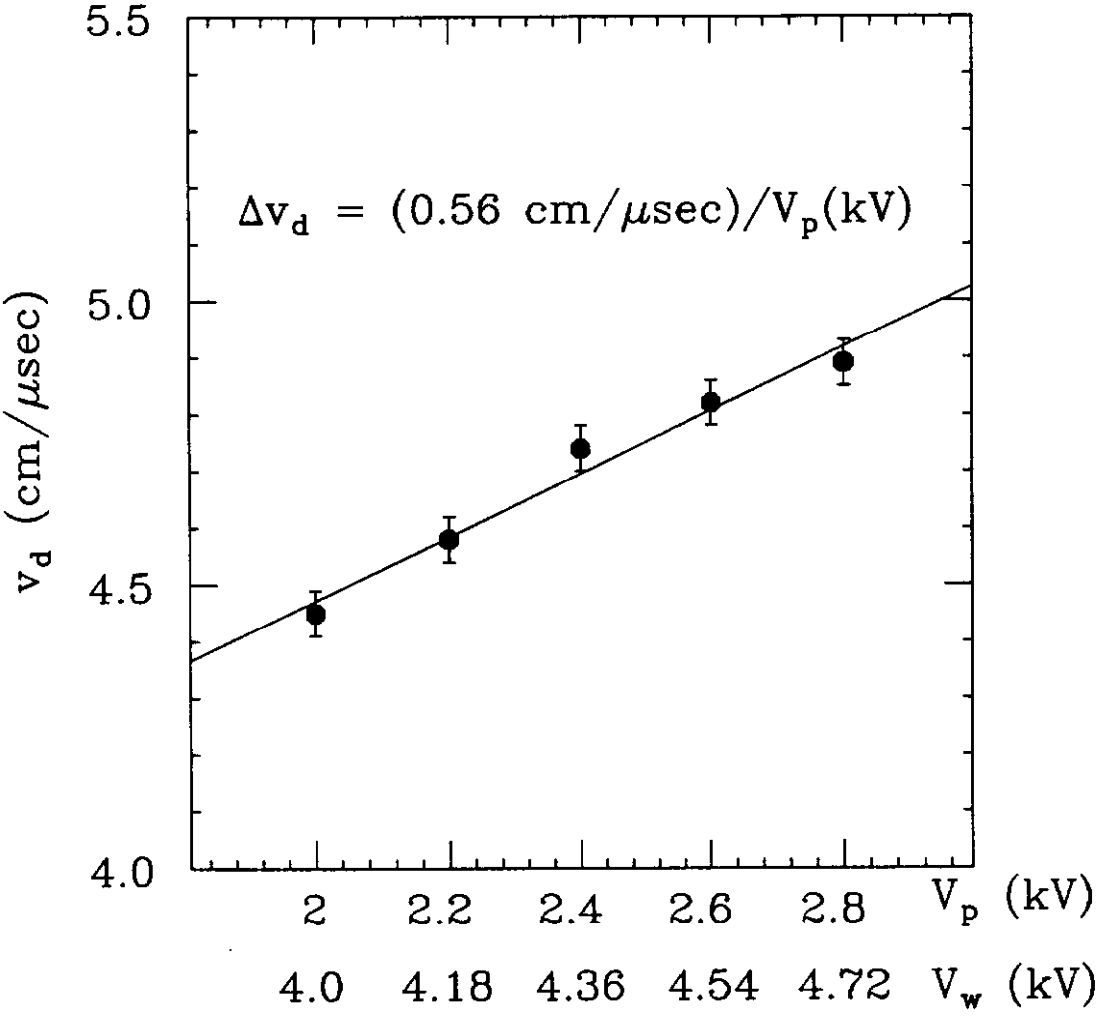
5.5
5.0
4.5
4.0
v_d (cm/μsec)
Δv_d = (0.56 cm/μsec)/V_p(kV)
2
2.2
2.4
2.6
2.8
V_p (kV)
4.0
4.18
4.36
4.54
4.72
V_w (kV)

Figure 9.

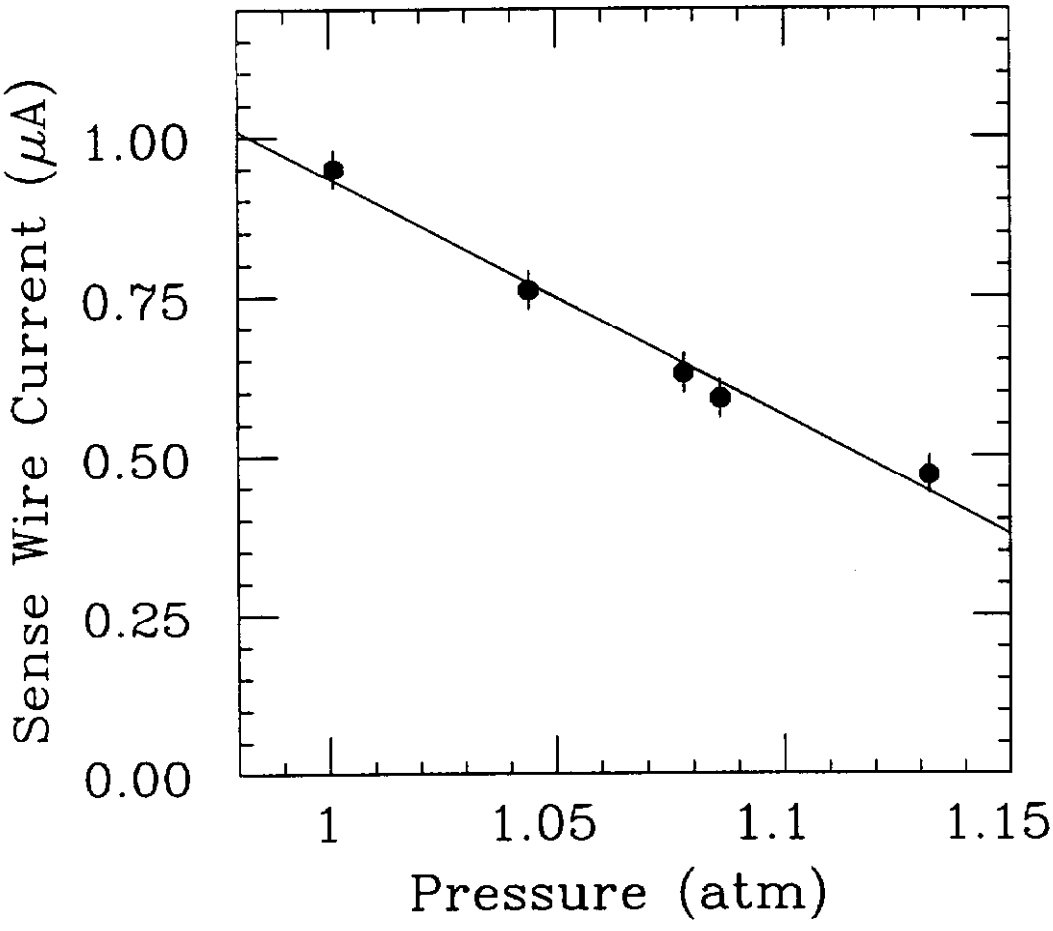
Sense Wire Current (μA)
1.00
0.75
0.50
0.25
0.00
1
1.05
1.1
1.15
Pressure (atm)

Figure 10.

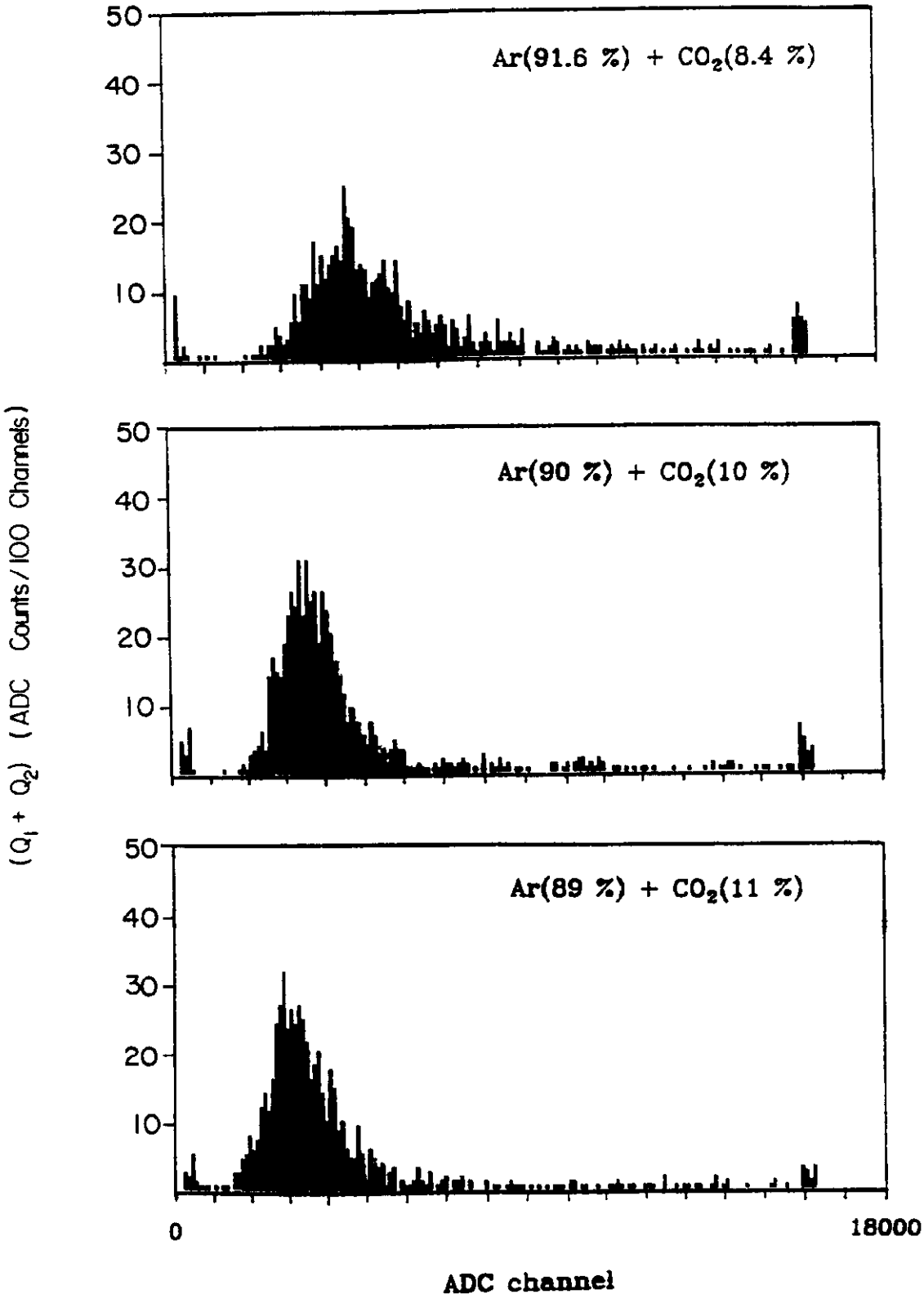
Ar(91.6 %) + CO_2(8.4 %)
Ar(90 %) + CO_2(10 %)
Ar(89 %) + CO_2(11 %)
50
40
30
20
10
$(Q_1 + Q_2)$ (ADC Counts / 100 Channels)
0
18000
ADC channel

Figure 11.

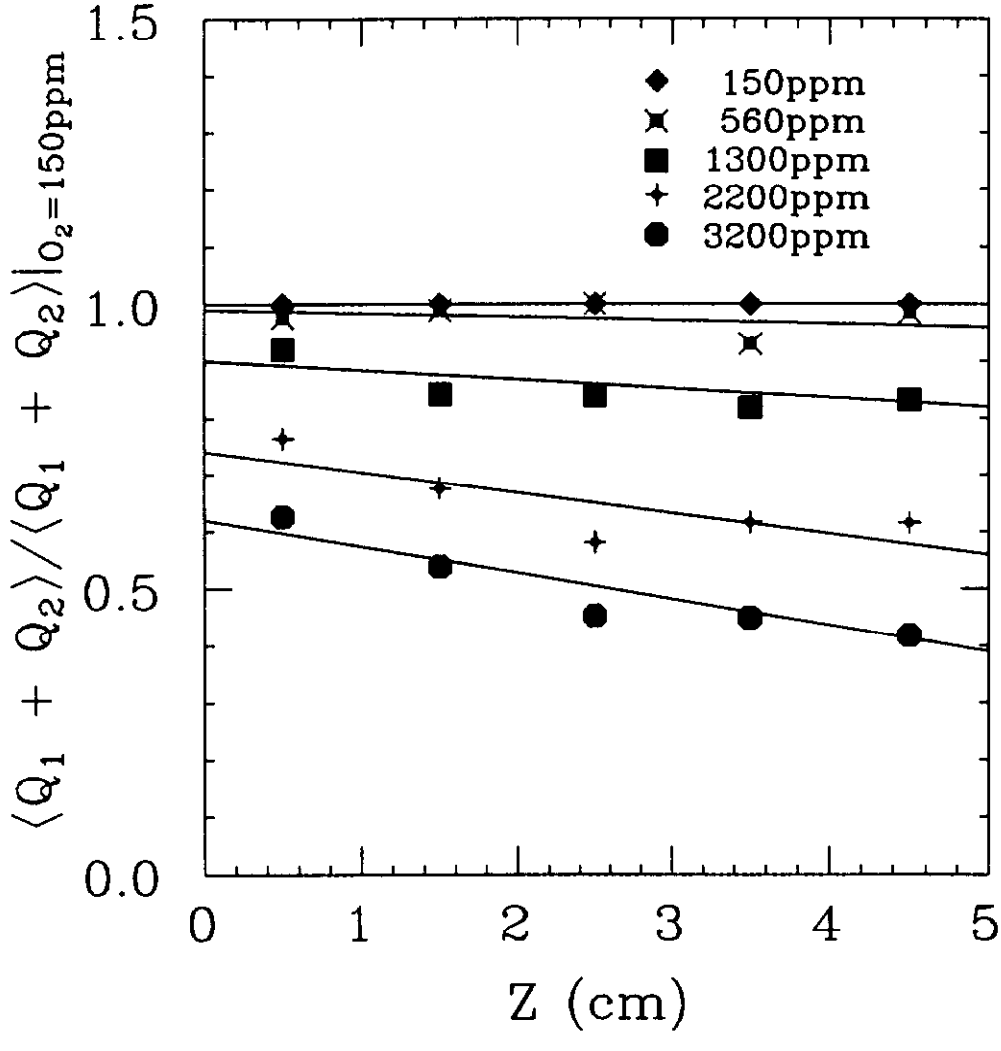
1.5
1.0
0.5
0.0
0
1
2
3
4
5
Z (cm)
$\langle Q_1 + Q_2 \rangle / \langle Q_1 + Q_2 \rangle|_{O_2=150ppm}$
150ppm
560ppm
1300ppm
2200ppm
3200ppm

Figure 12.

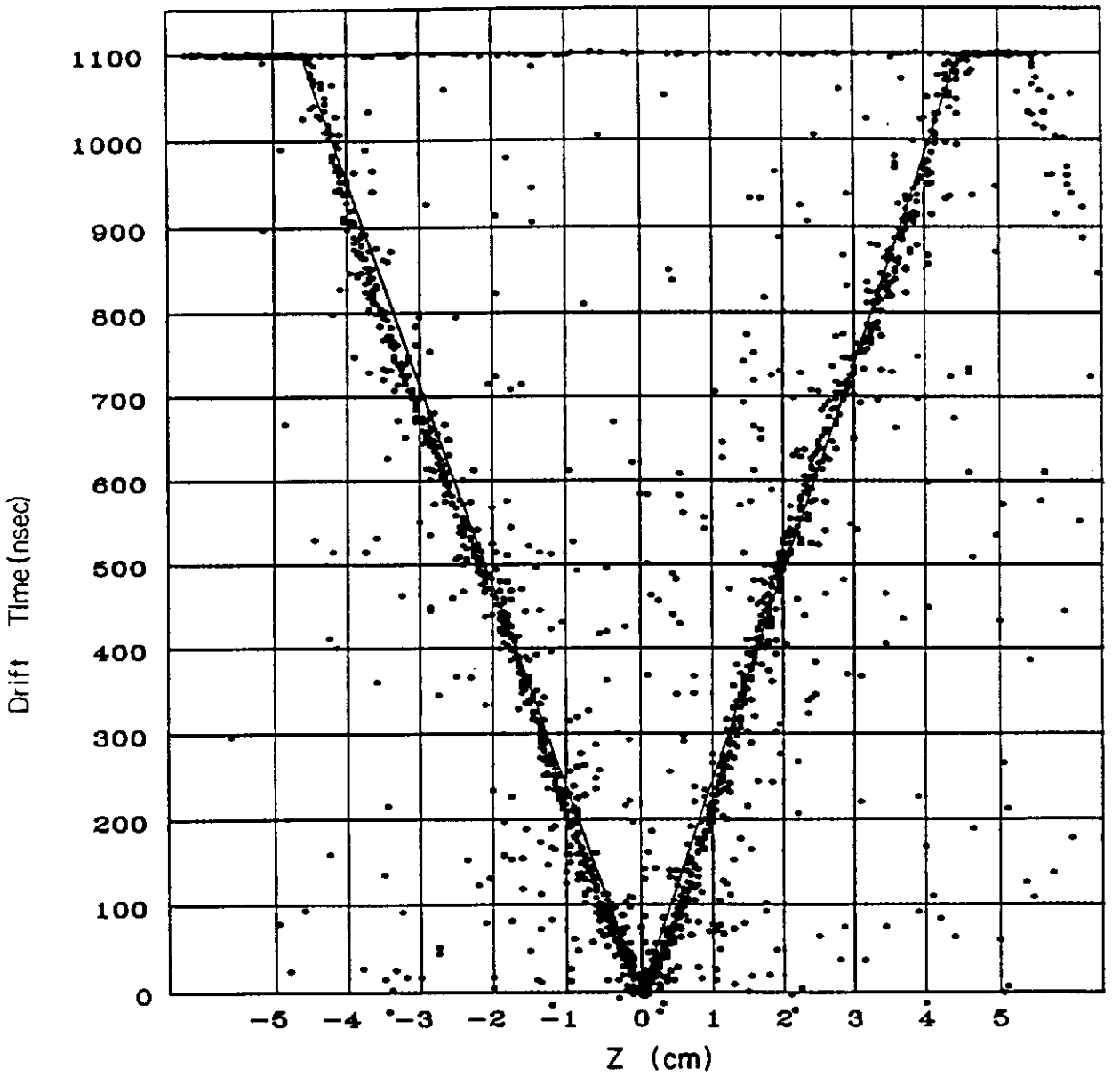
1100
1000
900
800
700
600
500
400
300
200
100
0
Drift Time (nsec)
−5
−4
−3
−2
−1
0
1
2
3
4
5
Z (cm)

Figure 13.

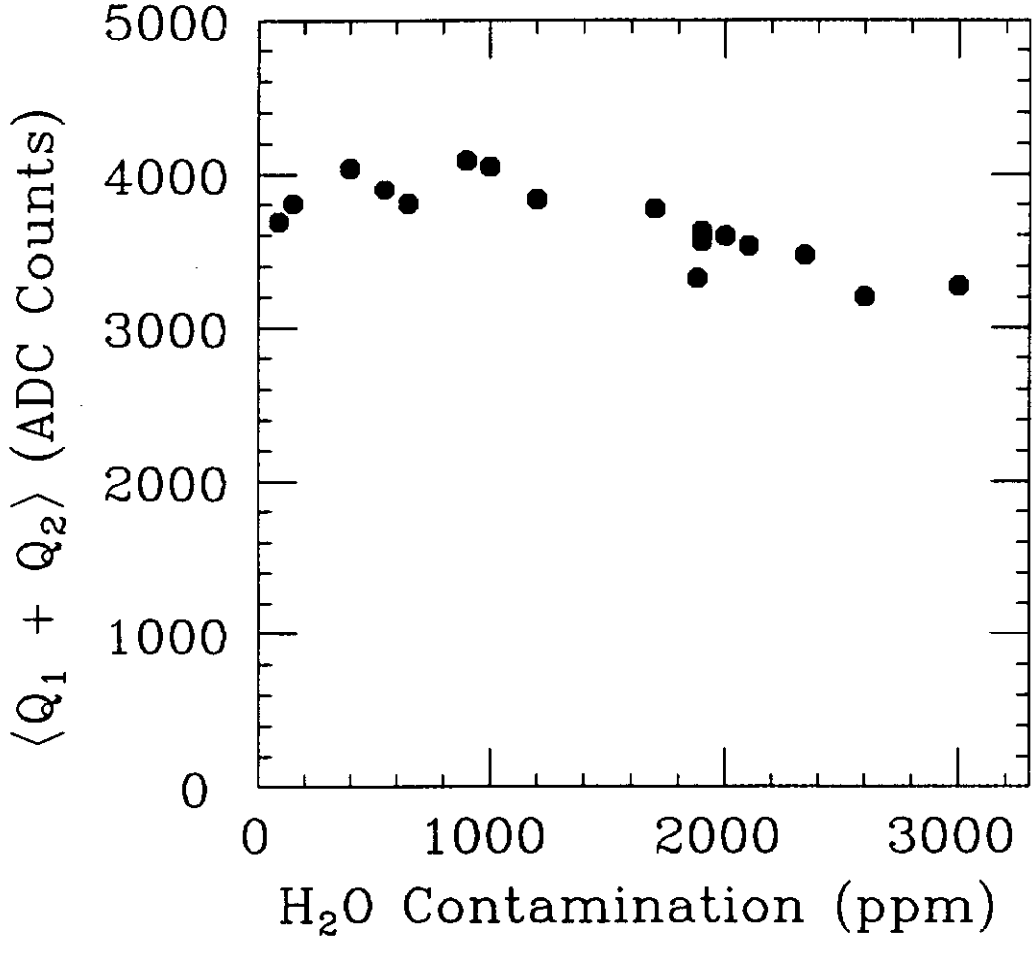
5000
4000
3000
2000
1000
0
0
1000
2000
3000
$\langle Q_1 + Q_2 \rangle$ (ADC Counts)
H_2O Contamination (ppm)

Figure 14.